# SELF-CONSISTENT LONG-TERM DYNAMICS OF SPACE CHARGE DRIVEN RESONANCES IN 2D AND 3D

Ingo Hofmann and Adrian Oeftiger*
GSI Helmholtzzentrum für Schwerionenforschung GmbH, Darmstadt, Germany
Oliver Boine-Frankenheim, Technische Universität Darmstadt, Darmstadt, Germany

## Abstract

Understanding the 3D collective long-term response of beams exposed to resonances is of theoretical interest and essential for advancing high intensity synchrotrons. This study of a hitherto unexplored beam dynamical regime is based on 2D and 3D self-consistent particle-in-cell simulations and on careful analysis using tune spectra and phase space. It shows that in Gaussian-like beams Landau damping suppresses all coherent parametric resonances, which are of higher than second order (the "envelope instability"). Our 3D results are obtained in an exemplary stopband, which includes the second order coherent parametric resonance and a fourth order structural resonance. They show that slow synchrotron oscillation plays a significant role. Moreover, for the early time evolution of emittance growth the interplay of incoherent and coherent resonance response matters, and differentiation between halo and different core regions is essential. In the long-term behaviour we identify a progressive, self-consistent drift of particles towards and across the resonance, which results in effective compression of the initial tune spectrum. However, no visible imprint of the coherent features is left over, which only control the picture during the first one or two synchrotron periods. An intensity limit criterion and an asymptotic formula for long-term rms emittance growth are suggested. Comparison with the commonly used non-self-consistent "frozen space charge" model shows that in 3D this approximation yields a fast and useful orientation, but it is a conservative estimate of the tolerable intensity.

## INTRODUCTION

Beam intensity in operating or future high intensity circular hadron accelerators is limited by space charge effects on resonances [1]. Contrary to low intensity operation, where resonances are single particle phenomena, high intensity requires self-consistent treatment with differentiation between incoherent and coherent resonance effects as well as consideration of Landau damping of nonlinear coherent parametric resonances. Analytical or semi-analytical models of the latter do not exist – in contrast to the rich literature on impedance driven dipole modes –, hence we depend largely on simulation and careful theory-based interpretation.

Long-term space charge effects on synchrotron resonances have been measured in dedicated campaigns (see, for example, Refs. [1–3]). Comparison with simulation models is essential for understanding resonant processes and min-imizing their effects on beam quality; but so far – for cpu and noise related reasons – only non-self-consistent "frozen space charge models" (FSM) have been employed in these campaigns, which require modeling of $10^5...10^6$ machine turns. Such fully self-consistent 3D simulations using large numbers of simulation particles and many turns of synchrotron lattices are quite possible. Examples are long-term studies of the Montague resonance with the IMPACT code [4], or recent work on parametric Landau damping using the SYNERGIA code [5].

Recently, coasting beam 2D studies in relatively short systems (hundreds of cells rather than hundreds of thousands) have been used as basis for conjectures on coherent resonance effects and suggestion of new types of synchrotron resonance charts based on assumed coherent shifts, with partly controversial conclusions (see Ref. [6], also Refs. [7, 8]). The need for *long-term* and self-consistent 3D studies to adequately address these issues becomes obvious.

Historically, Smith [9] first pointed out in the early 1960's that coherent effects on gradient error resonances should result in higher intensity; followed by Sacherer [10] who extended the concept of coherent shifts to nonlinear resonances in a 1D Vlasov-Poisson study. In the 1990's, the suggestion by Smith was partly confirmed in relatively short-term simulations by Machida [11]; a Vlasov model presented coherent frequencies in 2D including anisotropy [12], and a review article by Baartman [13] further advocated for the coherent shift concept. The distinction between coherent and incoherent second order resonance effects was studied experimentally in HIMAC [14] and the PSR [15].

In high intensity linear accelerators the theoretically predicted structural space charge resonance effects [16] got verified experimentally by detailed phase space diagnostics [17].

In circular accelerators space charge resonant effects are known to exist; however, distinguishing them from often dominating externally driven resonances and other machine specific effects continues to be a challenging issue for performance optimization of high intensity synchrotrons [18–21]. Besides studies in operating linear accelerators and synchrotrons, compact linear Paul trap devices are also used to explore – experimentally and theoretically – incoherent and coherent resonances in periodic focusing and 2D [22].

For high intensity hadron circular accelerators – different from linear devices – a main beam dynamics challenge is self-consistent and long-term 3D modelling including synchrotron oscillation, which has motivated the present study. As an exemplary case we choose a simple FODO cell for

---

* a.oeftiger@gsi.de

transverse periodic focusing and study primarily – with exceptions in 2D – the space charge induced resonances above 90°, the so-called 90° stopband of periodic focusing. It combines a fourth order structure resonance with the second order parametric resonance – the envelope instability – and thus allows studying the interplay of incoherent and coherent resonance.

We proceed with a short theory overview in Section , followed by a detailed 2D simulation analysis of different stopbands, Landau damping and incoherent core resonances in Section . In Section  we compare long-term 2D with 3D PIC simulation; Section  discusses the "frozen space charge modeling" (FSM) in 2D and 3D, Section  discusses possible applications and Section  presents conclusions and a brief outlook.

## THEORETICAL BACKGROUND

In circular accelerators it is common practice to describe the effect of space charge in terms of an incoherent footprint on resonance charts, which depends on the distribution function – besides chromatic and other effects not in the focus here. Equally wide-spread is the assumption that resonance analysis should be based on avoiding major resonance lines - defined in the absence of space charge - to intercept with this incoherent footprint. Such a picture cannot adequately account for self-consistent and possibly existing coherent resonant response beyond incoherent behaviour. This Section reviews some basic definitions and notions useful for the further discussion.

In a periodic and linear focusing lattice – ignoring bending – the single particle equation of motion in $x$ (and similar in $y, z$) along distance $s$ can be written as

$$x'' + K_x(s)x - \frac{q}{mc^2\beta^2\gamma^3}E_x(x, y, z, s) = 0, \qquad (1)$$

where the electric field from space charge is assumed nonlinear. For a matched beam it modifies the focusing and includes the space charge contribution from the whole ensemble of particles - also due to coherent effects - subject to self-consistent modeling. It is convenient to describe the FODO focusing by $k_{xy}$ as single particle transverse phase advance per FODO cell. It includes the space charge shift due to the linear part of the electric field, which reduces the zero-intensity phase advance $k_{0xy}$, with a dependence on amplitude due to nonlinear terms in the electric field. As an example, and using the ring-specific nomenclature of "tunes", the SIS18 at GSI includes $N = 12$ cells of periodic focusing, and a typical vertical $k_{0y} = 96°$ amounts to a tune of $Q_{0y} \equiv Nk_{0xy}/360° = 3.2$. In the remainder of our discussion the variation of focusing strength per cell is described by phase advances, while "tunes" is kept in general terms.

For simplicity, we restrict the present discussion also to symmetric phase advances and emittances in $x$ and $y$; machine specific studies relating to a broader range of parameters and lattice configurations are left to future works.

In the remainder of our discussion the usual "tunes" as phase advances per turn are replaced by the phase advances

per cell, thus emphasizing the focus on the stopband around 90° as well as its higher order counterparts at 60° and 45°.

### Incoherent and Coherent Resonance Conditions

As transverse incoherent resonance condition – refraining from coupling – can be written as

$$mk_{xy} = h\,360°, \qquad (2)$$

which is used here to characterize space charge driven incoherent structure resonances. Here $m$ is the resonance order and $h > 1$ describes a possible higher harmonic of the driving lattice structure term (with $h = 1$ in all following simulation examples). This is equivalent to $mQ_{xy} = h\,N$ in circular notation with $N$ cells per turn. The term *incoherent* is meant to describe the resonance response as single particle behaviour in the presence of a space charge force from an assumed matched beam distribution. It is essential to distinguish the spectral distribution $k_{xy}$ from $\bar{k}_{xy}$, the space charge shifted value of phase advances of an rms-equivalent KV beam. As usual, this shift is described in rms-equivalence as $\Delta\bar{k}_{xy} \equiv k_{0xy} - \bar{k}_{xy}$. In 3D bunches $\Delta\bar{k}_{xy}$ refers to the longitudinal bunch center, i.e. half the maximum phase advance shift for a Gaussian distribution.

This incoherent shift is also used to characterize the strength of coherent effects. For the latter, the distribution as a whole is assumed to deviate from its matched configuration by adopting a coherent mode structure, which induces a specific coherent frequency shift $F_m$. The question of whether such coherent effects actually exist for other than KV-distributions will be discussed further below. Assuming their existence, a coherent structure resonance condition can be formally written in the form:

$$m(\bar{k}_{xy} + F_m\Delta\bar{k}_{xy}) = \frac{h}{2}360°, \qquad (3)$$

where we use the notation of Ref. [23], which is based on evaluating dispersion relations from the Vlasov model of Ref. [12] (an alternative definition replacing $\bar{k}_{xy}$ by $\bar{k}_{0xy}$ is used in Ref. [24], and in analogous manner in Ref. [6]). Note that the corresponding circular notation is again obtained by replacing all $k$ by $Q$ and 360° by $N$. The resonance order is given by $m$, which also describes the order of a coherent mode pattern. The $F_m$ characterize the extra coherent shift depending on the mode, respectively resonance order, and in general on the ratios of focusing strengths and emittances. $h$ is an integer as before, but now $h = 2$ stands for the fundamental lattice harmonic, and higher even numbers for multiples thereof. Of special interest in this study is the case $h = 1$ (generally all odd numbers). This coherent half-integer – here also called 1:2 – mode describes the parametric resonances to be discussed further on.

### Parametric Resonances

These coherent parametric resonances – as a special case of coherent resonances – have originally been introduced in the 2D Vlasov perturbation analysis of KV distributions in periodic focusing in Ref. [25]. They were called

"180-degree" modes describing their half-integer nature and shown to exist from second to at least sixth order. The more widely used terminology of parametric resonances was later suggested in the 1D Vlasov analysis of a waterbag-type sheet beam of Ref. [26]. Note that the equivalent term "parametric instability" is also applied here. It is equally used for the "Mathieu instability" of particles propagated at 180° phase advance in periodic focusing [27] – the single-particle analogue to the unstable coherent modes considered here.

In both cases the exponential growth is enforced by the periodic focusing force varying at twice the eigenfrequency of the particle, respectively coherent mode. In the coherent parametric case the transverse oscillation mode characterized by the order $m$ in Eq. (3) determines the oscillation frequency of the coherent part of the electrical field term in Eq. (1), which in turn provides the resonance driving term. The parametric nature of this mechanism materializes through the periodical modulation of the focusing force, which pumps energy into the beam eigenmode and results in exponential growth – as opposed to non-parametric resonances. The term "instability" actually appears justified in view of the fact that initially the driving term of order $m$, along with an odd $h$ in Eq. (3), exists in the electric field term only on the noise level. This is different from the structure space charge resonances with only even $h$ – for example the $m$=4 case in Section –, which require the presence of a driving term in the initial (matched) beam. In spite of this physical justification we continue with the widely used terminology "parametric resonance" in the remainder of this paper. Obviously this parametric picture also applies to the $m$=2 envelope mode starting from initial noise or slight mismatch of the $h$=1 periodicity; here we keep the notation "envelope instability" as commonly used in accelerator literature.

More recently, the 2D KV Vlasov basis was broadened by generalizing the analysis of Refs. [12, 25] to combine the effects of periodic focusing with different focusing strengths and emittances in the two transverse planes [28].

These and all other Vlasov models of higher than first order (dipole) transverse modes have in common the absence of incoherent tune spread – apparently due to the mathematical difficulties to handle non-KV distributions with tune spreads. As a result, none of these analytical models includes the possibility of Landau damping, and computer simulation is needed. Nonetheless, results from KV-based Vlasov perturbation analysis are a useful tool to interpret simulation results with more realistic beam models.

## SHORT-TERM 2D SIMULATION RESULTS

To elucidate the interplay of incoherent and coherent resonance effects we start from 2D and focus on different stopbands of structure type resonances driven by space charge itself [29]. Magnet driven resonances with space charge are closely related, but left to future studies.

*Simulation of Stopbands*

For the 2D simulations we use the TRACEWIN PIC code [30] with 128.000 particles and $\Delta \bar{k}_{xy}$ kept constant at 12°. Waterbag distributions are compared with (uncorrelated) Gaussian distributions, which are truncated at $3.4\sigma$ throughout this study. Fig. 1 shows the relative rms emittance growth after 300 FODO cells versus $k_{0xy}$ for the 90° stopband. The sharp space charge shifted peak for an initial
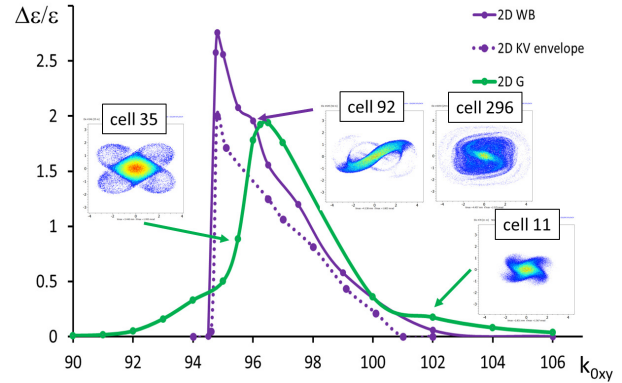


Figure 1: Rms emittance growth versus $k_{0xy}$ for the stopband above 90° for 2D waterbag and Gaussian distributions after 300 FODO cells. Inserts showing $x - x'$ phase space at different $k_{0xy}$ and cells.

waterbag distribution is due to the $m$=2 parametric resonance – the envelope instability – according to Eq. (3) (see inserts at cell 92 and 296), which coincides with the peak of the same mode obtained by the KV envelope equation. The initial Gaussian case shows a similar though somewhat weaker coherent response. The softer shoulders of the stopband reflect in addition an $m$=4 incoherent response according to Eq. (2). It is apparently driven by the structure type pseudo-octupole term of the space charge potential as confirmed by the four-fold symmetry in the inserts: at cell 35 for $k_{0xy} = 95.5°$ at the lower tune side; and a less pronounced one at cell 11 for $k_{0xy} = 102°$ (equivalent to $\bar{k}_{xy} = 90°$). Note that the absence of emittance growth for $k_{0xy} < 91°$ is owed to the truncation of Gaussian tails.

The 60° waterbag stopband in Fig. 2 gives a weaker response for the nonlinear $m$=3 parametric resonance with only 40% emittance growth (insert cell 225). For the Gaussian this mode is entirely absent; instead, a tiny ($< 0.8\%$) rms emittance growth due to a sixth order $m$=6 incoherent resonance driven by the structure pseudo-dodecapole of the space charge potential is found (insert cell 41). The 45° stopband in Fig. 2 shows the $m$=4 parametric resonance (insert cell 245), which reaches an rms emittance growth of only 2% for the waterbag and no detectable growth for the Gaussian case.

*Landau Damping of Parametric Resonances*

All in all, in 2D we find parametric resonances of second, third and fourth order to exist in the waterbag distribution, but only the second order mode in the Gaussian case. We
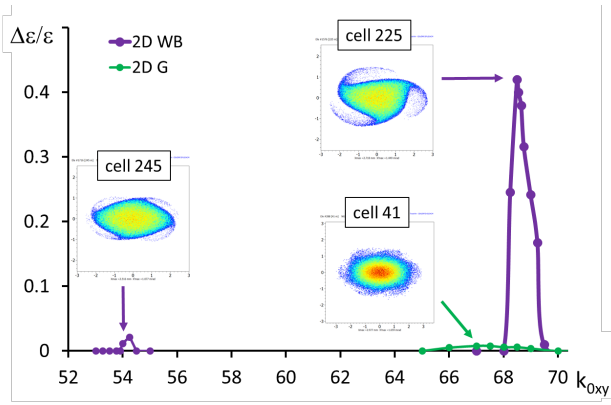
Figure 2: Rms emittance growth versus $k_{0xy}$ for the stop-bands above 60° and 45° for 2D waterbag and Gaussian distributions after 300 FODO cells. Inserts showing $x - x'$ phase space at different $k_{0xy}$ and cells.

explain this by Landau damping using the tune spectra extracted from self-consistent TRACEWIN simulations. In Fig. 3 the working point $k_{0xy} = 90°$ is chosen to obtain resonance-free spectra $f_0(k_{xy})$ representative for an initial beam situation at arbitrary $k_{0xy}$. Particle trajectories over $2^{14}$ elements (1820 cells with 9 elements per cell) are evaluated for this purpose. The coherent shifts following Eq. (3) (divided by $m$) are determined here from the peaks of respnse in the waterbag simulations in Figs. 1 and 2, indicated in Fig. 3 by colored lines. They can be compared with the corresponding $F_m$ obtained analytically from the 2D KV-based Vlasov analysis. For symmetric beams the highest frequency branches yield coherent factors decreasing with increasing $m$: $F_2 = \frac{1}{2}; F_3 = \frac{1}{4}; F_4 = \frac{3}{16}$ [23]. These theoretical values for the $F_m$ agree excellently with the waterbag simulations for $m=2$, but are about 30% lower for $m=3, 4$.

For Landau damping, an overlap in a region with $\partial f_0/\partial k_{xy} < 0$ is a necessity, which enables energy transfer from the coherent mode to the incoherent spectrum. For the waterbag beam none of the parametric modes $m=2, 3, 4$ satisfies this condition. For the Gaussian the $m=3, 4$ modes
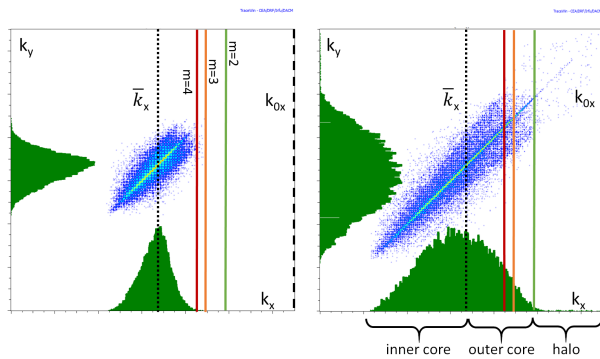


Figure 3: Spectral distributions $f_0(k_{xy})$ (as unnormalized intensity (per bin of $k_{xy}$) for 2D waterbag (l.h.s.) and Gaussian (r.h.s.) distributions generated for a fixed $k_{0xy}$. Also shown are locations of $\bar{k}_x$ and of the $m=2, 3, 4$ coherent mode lines (i.e. mode frequencies divided by $m$).

well satisfy it, which explains their suppression in Fig 2. The $m=2$ envelope instability overlaps only marginally – consistent with its instability. It can be assumed that the trend of decreasing $F_m$ for higher $m$ continues beyond $m=4$, which is supported by analytical expressions for 1D sheet beams in Ref. [26], and Landau damping should equally be expected.

*Incoherent Core Resonances*

It is helpful to divide the spectra in Fig. 3 into three spectral *tune regions*: an *inner core* with $\partial f_0/\partial k_{xy} \geq 0$; it transitions to an *outer core* with $\partial f_0/\partial k_{xy} < 0$ at $\bar{k}_{xy}$; and a *halo region*, where $f_0(k_{xy}) = 0$. For the resonance response it is essential in which tune region the resonance condition (here 90°) falls. Applied to Fig. 1: for $k_{0xy}$ from 90 ... 95° this occurs in the halo region; from 95 ... 102° in the outer core; and from 102 ... 114° in the inner core region.

The main characteristic of the Eq. (2) incoherent resonances is their local excitation in the tune spectrum. Their existence even in the beam core is verified in Fig. 4 for a Gaussian distributions and two different working points $k_{0xy}$. For $k_{0xy} = 102°$ the $4k_{xy} = 360°$ resonance condition (see
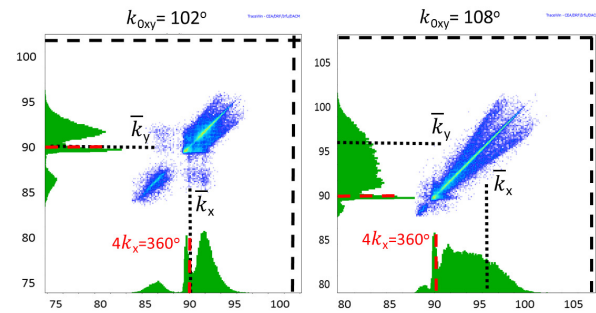


Figure 4: Spectral tune distributions for 2D Gaussian distributions with incoherent 4th order resonances in the beam core.

also insert cell 11 in Fig. 1) coincides with $\bar{k}_{xy}$ – the transition from outer to inner core. The gap opening up in the tune spectrum below 90° indicates a drift of particles towards and across the resonance, which progresses self-consistently due to the resulting density dilution in the inner core. We find an overall minor rms emittance growth of about only 10% over 3000 cells.

In the inner core region illustrated by the $k_{0xy} = 108°$ case in Fig. 4 the situation differs. We find again a clear resonance imprint on the tune spectrum, but only negligible rms emittance growth.

## LONG-TERM 2D AND 3D SIMULATION

The 2D results shown in Figs. 1 and 2 suggest that parametric resonance only matters for the $m=2$ mode, e.g. envelope instability in Eq. (3). This resonance occurs in the 90° stopband, which is the reason for focusing on this particular stopband in the following.

The code basis of SixTrackLib [31] and PyHEADTAIL [32] is used to simulate the long-term behaviour with full 3D PIC [33], which also allows 2D simulations for comparison.
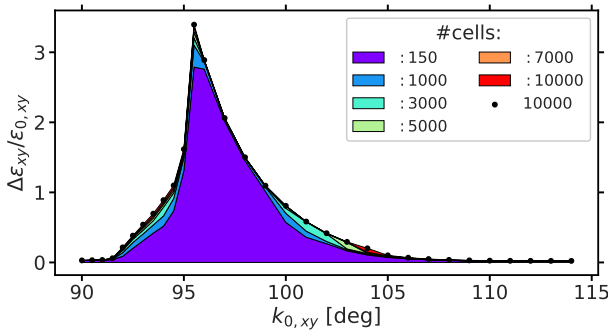
(a) Self-consistent 2D PIC simulation.
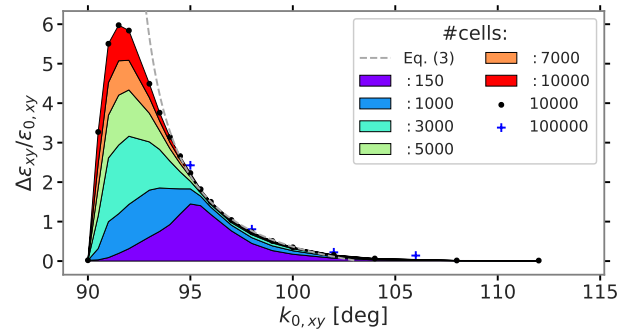


(b) Self-consistent 3D PIC simulation.

Figure 5: Long-term PIC simulations. Rms emittance growth versus $k_{0xy}$ for different total numbers of FODO cells.

The same tools are also used for the FSM calculations in Section . By employing GPU hardware for high-performance computation, a high resolution of 4 million macro-particles were tracked in only a few hours on a 3D grid of transversely 256×256 and longitudinally 64 cells, limiting grid heating effects to below permille level over the simulations. In order to focus on transverse space charge effects in a 3D bunch including realistic synchrotron motion time scales, parameters are chosen such that longitudinal space charge is reduced to a negligible level. The bunch length is kept small compared to the RF period such as to remain in the linear synchrotron motion regime.

## 2D Simulation Results

Figure 5a shows the rms emittance evolution for working points above the 90° resonance, with shaded areas relating to the rms emittance value after the indicated number of FODO cells. The purple area corresponds to the early short-term behaviour, which reproduces the same features as observed in TRACEWIN (cf. the green curve in Fig. 1): a peak around 96° is shaped by the coherent response of the space charge shifted envelope instability, with shoulders of incoherent resonance response on both sides.

The following evolution of the rms emittance until 10000 FODO cells reveals limited additional growth for the 2D problem. In particular, the tune region directly above 90° remains at weak emittance growth, where only the halo particles – limited by the truncation of Gaussian tails – are affected by the incoherent resonance. No particles are fed into the resonance once the halo region is depleted. We note that the long-term 2D behaviour of coasting beams is thus mainly characterized by the absence of synchrotron oscillations, which will be contrasted by the next section on 3D dynamics.

## 3D Simulation Results

In elongated 3D bunched beams the additional synchrotron oscillation effect is significant [34, 35]. It leads to a periodical crossing of resonance islands through the orbits, and trapping of particles occurs, if the motion of the island is slow with regard to the period of revolution around the fixed point. As shown in Ref. [35] this is more likely to occur for smaller synchrotron amplitudes, whereas large amplitudes may result in a sequence of small jumps of the single-particle emittance ("scattering"). The relative importance of trapping or scattering depends on the strength of the resonance and the synchrotron period.

Note that in this Section we assume 3D uncorrelated Gaussian distributions and use the same lattice and other parameters as in 2D simulations. Figure 5b shows the rms emittance evolution at the slowest synchrotron oscillation in our study – a ratio of 1:300 for betatron to synchrotron period. The same contour levels of rms emittance evolution are plotted like in Fig. 5a. As opposed to the latter 2D case, where only effects related to short-term dynamics are observed (the upper edge of the violet 150-cells region almost coincides with the black dotted 10000-cells contour), the 3D case reveals significant long-term dynamics.

In the halo region 90 ... 95°, the emittance growth due to the fourth-order incoherent resonance is much enhanced due to the synchrotron oscillation. We argue that due to the relatively strong space charge resonance the synchrotron period chosen in our simulation is already slow enough to have a dominant part of particles in the trapping regime. This is supported by the observation that a single synchrotron period (1200 cells) already shows a substantial increase of the rms emittance in Figure 5b. A strong growth is visible already after 150 FODO cells (1/8th synchrotron period). This effect significantly continues with the number of FODO cells, while the peak of the emittance growth curve shifts more and more down towards $k_{0xy} = 90°$.

The transition from halo to the outer core lies in the region around $90° + \Delta\bar{k}_{xy}/2 \approx 96°$, where the peak of the envelope instability is encountered in the early evolution (cf. violet area). Eminent coherent motion in phase space as well as in the coherent spectrum is identified, which vanishes after a few 100 turns. At the same time, in all of the outer core (similar to the halo) particles at large transverse amplitudes are found to be driven into a four-fold symmetric island structure: an imprint of the incoherent $m=4$ resonance in accordance with 2D in 4 . In contrast to the halo region, rms emittance growth effectively stops after about 150 turns and the dynamics is largely independent of the synchrotron motion time scale.

The inner core region beyond the point $k_{0xy} = 102°$ in Fig. 5b, where $\bar{k}_{xy}$ crosses the 90° resonance from below, is characterised by negligibly small emittance growth. We noted this important result already in the 2D treatment: although tunes are observed to accumulate around the resonance at 90° in the self-consistent simulations, there is little to no net effect on rms emittance growth.

To confirm the long-term behaviour in the outer and inner core region, selected simulation cases have been run for an order of magnitude longer: the blue crosses in Fig. 5b mark the rms emittance growth values after 100000 FODO cells. Apart from a slightly increased rms emittance owing to the inherent noise effects of the PIC method such as grid heating, the blue crosses indeed match the black dots (marking the evolution after 10000 FODO cells). Therefore there is no evidence of additional significant resonance dynamics impacting the *rms emittance* beyond what is described above: the rms emittance growth has well saturated within 10000 turns in both outer and inner core $k_{0xy}$ regions.

The continuous emittance growth near the resonance $k_{0xy} = 90°$, on the other hand, would translate to losing the resonating particles in the halo region in the aperture of a real machine. Exact emittance growth figures beyond the structural behaviour described in the 10000 turns here are thus of less interest.

### 3D Asymptotic Emittance Growth

We use these observations to postulate an approximate long-term asymptote for the emittance evolution in the halo and outer core regions. It is based on the fact that the tune spread of a space charge dominated beam is inversely proportional to its rms emittance. Hence a comparison between the initial and expected final tune spread allows an estimate of the rms emittance growth factor. The final tune spread results from a geometrical argument: for $\bar{k}_{xy} < 90°$ the self-consistent, progressive drift of particle tunes across $k_{res} = 90°$ results in a final "compression" of tune space to the available width above resonance, $k_{0xy} - k_{res}$. The corresponding initial spread is $k_{0xy} - \bar{k}$, which allows to describe the relative growth by the asymptotic formula

$$\left(\frac{\Delta\epsilon}{\epsilon}\right)_{final} \approx \frac{k_{res} - \bar{k}_{xy}}{k_{0xy} - k_{res}} = \frac{\Delta\bar{k}_{xy}}{k_{0xy} - k_{res}} - 1. \quad (4)$$

It is applicable as long as $k_{res} > \bar{k}_{xy}$, or $k_{0xy} < k_{res} + \Delta\bar{k}_{xy}$; and no growth in the inner core region with $k_{res} < \bar{k}_{xy}$ consistent with Section .

A finite stop-band width would shift the effective $k_{res}$ to slightly above 90°. This margin can be used for an optimum fit to the 10000 cells simulation data of Fig. 5b in the range $k_{0xy} \geq 95°$, where saturation is approximately reached. With an effective $k_{res} = 91.2°$ the resulting hyperbolic asymptote is represented by the dashed gray line in Fig. 5b with a remarkably good match.

Note that the absence of further parameters in Eq. (4) suggests a general applicability to long-term resonance behavior dominated by large space charge tune spreads, also extending to externally driven resonances and beyond the 90° stopband, which warrants further study. Obviously, in a realistic machine the mechanical aperture would turn the continuous emittance growth for $k_{0xy} \rightarrow 90°$ into finite beam loss.

A striking insight from the present long-term study is the observed absence of eminent isolated emittance growth peaks relating to coherent resonance conditions, in particular for time scales as relevant for synchrotrons (i.e. beyond 1000 FODO cells).

### Halo vs. Core Dynamics

The difference between the slow incoherent regime in the halo $k_{0xy}$ region and the fast coherent regime in the outer core $k_{0xy}$ region can be illustrated using incoherent tune footprints. They are acquired via harmonic analysis over 512 FODO cells.

Figure 6a shows the halo case for $k_{0xy} = 92°$: the final tune footprint at 10000 FODO cells is plotted in black. The corresponding black histogram projections indicate that half of the particles have accumulated above the $k_{res} = 90°$ condition. The incoherent resonance causes a slow drift of particles across the resonant tune and the overall tune spread shrinks. The slow pace becomes apparent when comparing to earlier times in the simulation: the violet histogram corresponds to the situation after 150 FODO cells (like in Fig. 5b) and shows more than 85% of the particles situated below 90°. Some particles are resonating at 90° indicated by the growing peak there. The turquoise histogram corresponds to 3000 FODO cells where a third of the particles have moved above 90°.

Figure 6b depicts the outer core case at $k_{0xy} = 96°$. The black tune footprint at 10000 FODO cells indicates that most particles have been reallocated to above the resonance, a mere 6% are left below. In contrast to the previous halo scenario, the now present envelope instability has carried more than 80% of the particles to above the resonance already around 150 FODO cells, as can be seen in the violet histogram. This behaviour is illustrated in the simulation animation published as Ref. [36]. The coherent resonance mechanism does not distinguish transverse amplitudes, particles participate in the pumped mode across all transverse single-particle emittances simultaneously. Correspondingly, both the rms emittance and the individual particle emittances grow at the same time. After the parametric resonance has faded, the remaining particles at the lower end of the tune footprint (at small betatron amplitudes in the centre of the bunch) are slowly transported above 90° via the incoherent resonance mechanism.

The two simulation cases in the incoherent halo region as well as the outer core region with both coherent and incoherent resonance dynamics agree on the asymptotic state: the tune spread shrinks – either at slow or fast pace, respectively – until its lower end is located above the $k_{res} = 90°$ condition. This observation illustrates the asymptotic behaviour discussed in the previous section.

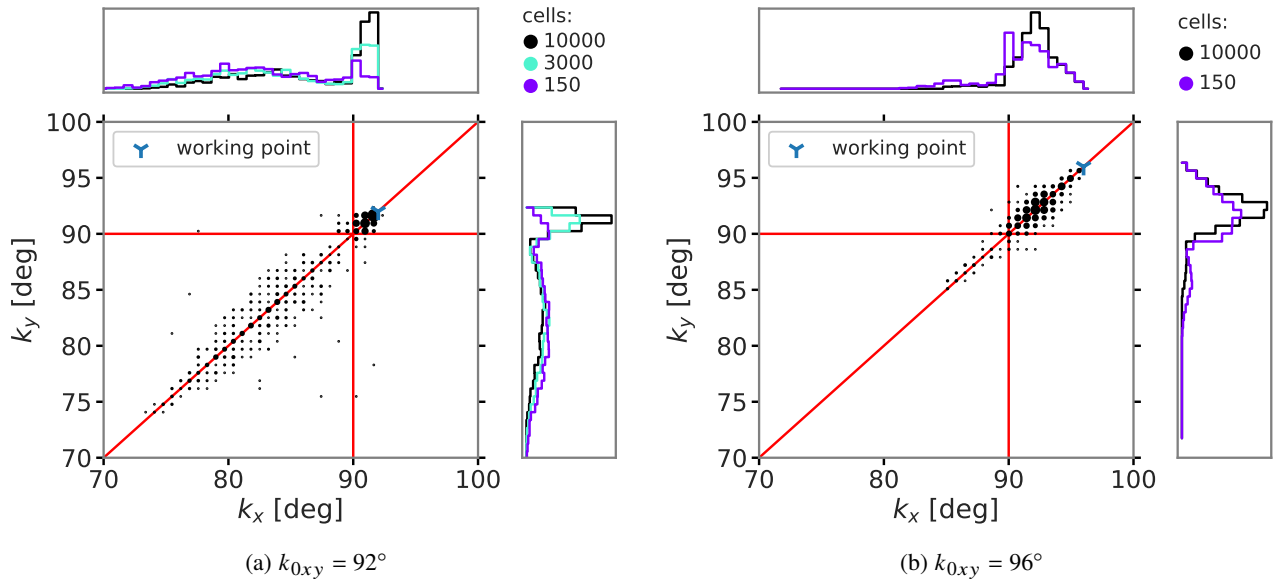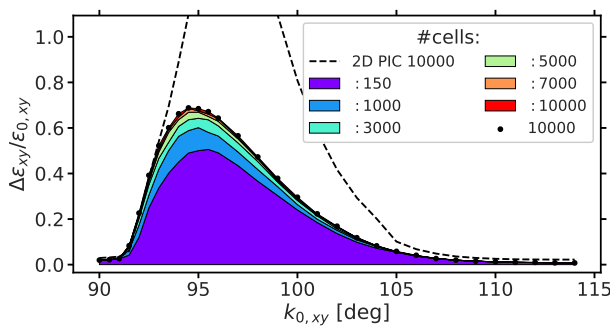(a) $k_{0xy} = 92°$                    (b) $k_{0xy} = 96°$

Figure 6: Tune footprints in halo and outer core region for 3D PIC simulation.

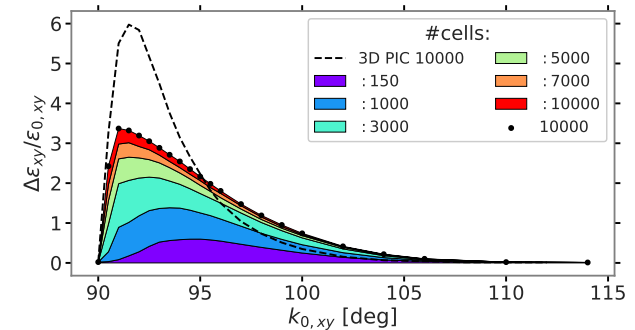## FROZEN SPACE CHARGE SIMULATION

In the last part we compare the previous self-consistent PIC computations to FSM, where the initial Gaussian beam space charge force is kept unchanged and macro-particles are merely treated as test particles not contributing to the space charge force dynamically, for otherwise identical parameters as for PIC in Section . The FSM by definition generates only incoherent response in all regions without self-consistent feedback. It thus allows to single out incoherent effects, where the full PIC simulation includes coherent effects as well as the self-consistent change of the distribution.

### 2D FSM

Figure 7a presents FSM results for coasting beam conditions. The black dots indicate the emittance growth from the frozen fieldmap treatment in FSM after 10000 FODO cells, which is saturated as there is almost no further emittance growth observed across the final 3000 cells. This result is to be compared with the 2D PIC simulations from Fig. 5a, where the final contour after 10000 FODO cells has been added here as a dashed line for reference.

In contrast to the FSM simulation, the self-consistent PIC treatment delivers strongly enhanced emittance growth in a tune interval between $94° \leq k_{0xy} \leq 105°$, where the $m=2$ envelope instability grows significantly. On the other hand, PIC and FSM predicted emittance growth matches very well on the left shoulder close to 90°, where the halo particles increase in amplitude only due to the incoherent fourth-order resonance driven by the octupole component of the space charge field from the resonance-free core.

### 3D FSM

Figure 7b presents FSM results to be compared with the PIC simulations in Fig. 5b. The PIC simulated 10000 FODO cells curve is included in dashed for reference.

In the halo region, we find reduced rms emittance growth due to the missing self-consistent tune drift towards the resonance in FSM. Over still longer times the dominating periodic resonance crossing effect through synchrotron motion appears to provide FSM results closer to the PIC simulations.

In the outer core region, the absence of coherent effects in the FSM leads to initially slower developing rms emittance



(a) 2D FSM computation (2D PIC in dashed).          (b) 3D FSM computation (3D PIC in dashed).

Figure 7: Long-term frozen simulations. Rms emittance growth versus $k_{0xy}$ for different total numbers of FODO cells.

growth. Final saturation, instead, occurs at a non-negligibly higher level due to the non-self-consistent nature of the space charge force in FSM. For synchrotron design applications, we conclude that the FSM tends to underestimate the area of working points with low-level emittance growth compared to PIC.

## DISCUSSION

The results of long-term simulations presented here have a number of implications for the choice of working points and intensity limits. They also shed light on the confidence level of FSM simulations, which are often the dominant simulation tool for evaluating synchrotron beam dynamics experiments.

The findings of Sections  and  suggest as criterion for negligible rms emittance growth that it is sufficient to keep the rms-equivalent KV tune above the resonance condition – here 90° – instead of the more restrictive "conventional" single particle assumption requiring the complete tune footprint above the resonance. This can be applied, for example, to the SIS18 at GSI with 12 lattice periods and $k_{0y}$ above 90°, hence $Q_{0y}$ above 3. From the point of view of the here discussed space charge driven second and fourth order structure resonances, the choice of a vertical $Q_{0y} = 3.25$ would still allow a maximum incoherent space charge tune spread of −0.5 in the center of a Gaussian beam – twice as large as assumed by the single particle arguments. This would similarly apply to the PS Booster at CERN with its 16 lattice periods.

The 2D comparison between FSM and PIC space charge modelling in Section  demonstrates that FSM underestimates emittance growth in the outer core region by a large factor, and by a smaller factor in the inner core region. The large factor is due to the existence of the envelope instability in the 90° stopband.

In 3D though, a long lasting emittance growth effect by this unstable mode is inhibited by synchrotron oscillation, which itself is also modelled by FSM as shown in Section . This qualifies the approximate 3D FSM treatment as a computationally effective tool for conservative identification of emittance conserving working points. On the one hand, the predicted finite emittance growth for resonance affected tune regions with FSM deviates quantitatively from PIC results: according to Fig. 7b FSM underestimates growth in the halo region, but overestimates it in the inner core region (at the very right) by more than a factor two. On the other hand, resonance-free tune regions computed via the fast FSM also remain resonance-free in the PIC case, which qualifies 3D FSM as conservative in all regions.

## CONCLUDING REMARKS

In summary, incoherent effects are found to play a major role in the long-term dynamics of bunches – not only in the beam halo but also in the beam core. Sufficient overlap with the incoherent spectrum in 2D is found to account for Landau damping of the $m > 2$ parametric resonances. In 3D, synchrotron oscillation is expected to even further en-

hance Landau damping – in analogy to studies of head-tail modes [37–39]. On the other hand, very short synchrotron periods comparable with betatron periods – as typical for near-spherical linac bunches – suppress the resonant mechanism of Landau damping [24, 29].

In the *halo region*, in our example at tunes slightly above 90°, synchrotron motion strongly enhances rms emittance growth due to incoherent resonance. In the adjacent *outer core region*, we stress the importance of the encountered self-consistent interplay between coherent and incoherent effects. Incoherent resonances emerge with particle tunes accumulating at the incoherent resonance condition (in our example $m$=4), and corresponding resonance islands form in phase space.

Our comparison between the 3D self-consistent and frozen treatments demonstrates that the early time evolution of rms emittance growth is largely determined by distribution change and coherent effects. Long-term saturation of rms emittance growth in 3D, however, is qualitatively determined by the compression of the entire incoherent tune footprint into the interval between bare tune and incoherent resonance condition as described by our asymptotic formula.

Thus, over times of long-term bunch storage, we find the overall rms emittance growth response curves in 3D to be smooth. Comparison of Fig. 5a with Fig. 5b confirms that even the strong envelope instability shows no coherent imprint after few thousand cells of 3D simulation (e.g. few synchrotron periods). This suggests that introducing parametric resonance lines to the synchrotron resonance charts introduced in Ref. [6] is relevant only for coasting beams in case of the $m$=2 envelope instability; furthermore for $m$>2 parametric resonances and such initial distributions, which are truncated to the extent that Landau damping does not work. Instead, we find the criterion that the $k_{0xy}$ region with non-negligible emittance growth spans from the resonant 90° to 90° + $\Delta \bar{k}_{xy}$, with final rms emittances determined by the tune footprint compression effect.

This study is expected to have an impact on future studies at various accelerators with the goal to extend and test the applicability of our conclusions to (a) higher-order resonances driven by space charge and (b) externally driven resonances in conjunction with space charge.

## REFERENCES

[1] H. Bartosik, "Challenges in Understanding Space Charge Dynamics", in *Proc. 61st ICFA Advanced Beam Dynamics Workshop on High-Intensity and High-Brightness Hadron Beams (HB'18)*, Daejeon, Korea, Jun. 2018, pp. 1–7. doi:10.18429/JACoW-HB2018-MOA1PL01

[2] G. Franchetti *et al.*, "Experiment on space charge driven nonlinear resonance crossing in an ion synchrotron", *Phys. Rev. ST Accel. Beams*, vol. 13, p. 114203, 2010. doi:10.1103/PhysRevSTAB.13.114203

[3] G. Franchetti, S. Gilardoni, A. Huschauer, F. Schmidt, and R. Wasef, "Space charge effects on the third order coupled resonance", *Phys. Rev. Accel. Beams*, vol. 20, p. 081006, 2017. doi:10.1103/PhysRevAccelBeams.20.081006

[4]  J. Qiang, R. D. Ryne, G. Franchetti, I. Hofmann, and E. Métral, "Numerical Simulation Study of the Montague Resonance at the CERN Proton Synchrotron", in *Proc. 3rd Int. Particle Accelerator Conf. (IPAC'12)*, New Orleans, LA, USA, May 2012, paper WEPPR011, pp. 2958–2960.

[5]  A. Macridin, A. Burov, E. Stern, J. Amundson, and P. Spentzouris, "Parametric Landau damping of space charge modes", *Phys. Rev. Accel. Beams*, vol. 21, p. 011004, 2018. doi:10.1103/PhysRevAccelBeams.21.011004

[6]  K. Kojima, H. Okamoto, and Y. Tokashiki, "Empirical condition of betatron resonances with space charge", *Phys. Rev. Accel. Beams*, vol. 22, p. 074201, 2019. doi:10.1103/PhysRevAccelBeams.22.074201

[7]  I. Hofmann, "Comment on 'Empirical condition of betatron resonances with space charge'", *Phys. Rev. Accel. Beams*, vol. 23, p. 028001, 2020. doi:10.1103/PhysRevAccelBeams.23.028001

[8]  K. Kojima, H. Okamoto, and Y. Tokashiki, "Reply to "Comment on 'Empirical condition of betatron resonances with space charge'"", *Phys. Rev. Accel. Beams*, vol. 23, p. 028002, 2020. doi:10.1103/PhysRevAccelBeams.23.028002

[9]  L. Smith, "Effect of gradient errors in the presence of space charge forces", in *Proc. of the 4th Intern. Conf. on High-Energy Accelerators*, edited by A. A. Kolomenskij and A. B. Kuznetsov, Dubna, USSR, 1963 , p. 1232.

[10]  F. J. Sacherer, Ph.D thesis, Lawrence Radiation Laboratory Report No. UCRL-18454, 1968.

[11]  S. Machida, "Space charge effects in low-energy proton synchrotrons", *Nucl. Instrum. Methods Phys. Res., Sect. A*, vol. 309, pp. 43–59, 1991. 10.1016/0168-9002(91)90091-4

[12]  I. Hofmann, "Stability of anisotropic beams with space charge", *Phys. Rev. E*, vol. 57, p. 4713, 1998. doi:10.1103/PhysRevE.57.4713

[13]  R. Baartman, "Betatron resonances with space charge", *AIP Conf. Proc.*, vol. 448, p. 56, 1998. doi:10.1063/1.56781

[14]  T. Uesugi, S. Machida, and Y. Mori, "Experimental study of a half-integer resonance with space-charge effects in a synchrotron", *Phys. Rev. ST Accel. Beams*, vol. 5, p. 044201, 2002. doi:10.1103/PhysRevSTAB.5.044201

[15]  S. Cousineau, J. Holmes, J. Galambos, A. Fedotov, J. Wei, and R. Macek, "Resonant beam behavior studies in the Proton Storage Ring", *Phys. Rev. ST Accel. Beams*, vol. 6, p. 074202, 2003. doi:10.1103/PhysRevSTAB.6.074202

[16]  D. Jeon, L. Groening, and G. Franchetti, "Fourth order resonance of a high intensity linear accelerator", *Phys. Rev. ST Accel. Beams*, vol. 12, p. 054204, 2009. doi:10.1103/PhysRevSTAB.12.054204

[17]  L. Groening *et al.*, "Experimental Evidence of the 90° Stop Band in the GSI UNILAC", *Phys. Rev. Lett.*, vol. 102, p. 234801, 2009. doi:10.1103/PhysRevLett.102.234801

[18]  F. Asvesta, H. Bartosik, A. Huschauer, and Y. Papaphilippou, "Space Charge Driven Resonances in the CERN PS", in *Proc. 10th Int. Particle Accelerator Conf. (IPAC'19)*, Melbourne, Australia, May 2019, pp. 3216–3219. doi:10.18429/JACoW-IPAC2019-WEPTS047

[19]  V. Kornilov, A. Oeftiger, O. Boine-Frankenheim,b, V. Chetvertkova, S. Sorge, and P. Spiller, "Beam quality and beam loss predictions with space charge for SIS100", *Journ. of Instr.*, vol. 15, p. P07020, 2020. doi:10.1088/1748-0221/15/07/P07020

[20]  H. Bartosik, F. Asvesta, A. Huschauer, Y. Papaphilippou, and F. Schmidt, "Space charge induced losses in the CERN injector complex", *Journ. of Instr.*, vol. 15, p. P07021, 2020. doi:10.1088/1748-0221/15/07/P07021

[21]  H. Hotchi *et al.*, "J-PARC 3-GeV RCS: 1-MW beam operation and beyond", *Journ. of Instr.*, vol. 15, p. P07022, 2020. doi:10.1088/1748-0221/15/07/P07022

[22]  H. Okamoto, M. Aoki, C. Ichikawa, K. Kojima, T. Kurauchi, and Y. Yamane, "Coherent and incoherent space-charge effects in high-intensity hadron rings", *Journ. of Instr.*, vol. 15, p. P07017, 2020. doi:10.1088/1748-0221/15/07/P07017

[23]  I. Hofmann, *Space Charge Physics for Particle Accelerators*, New York, NY, USA: Springer, 2017, p. 49.

[24]  I. Hofmann and O. Boine-Frankenheim, "Parametric instabilities in 3D periodically focused beams with space charge", *Phys. Rev. Accel. Beams*, vol. 20, p. 014202, 2017. doi:10.1103/PhysRevAccelBeams.20.014202

[25]  I. Hofmann, L.J. Laslett, L. Smith and I. Haber, "Stability of the Kapchinskij-Vladimirskij (K-V) distribution in long periodic transport systems", *Part. Accel.*, vol. 13, p. 145, 1983. http://cds.cern.ch/record/140869

[26]  H. Okamoto and K. Yokoya, "Parametric resonances in intense one-dimensional beams propagating through a periodic focusing channel", *Nucl. Instrum. Methods Phys. Res., Sect. A*, vol. 482, p. 51, 2002. doi:10.1016/S0168-9002(01)01684-9

[27]  M. Reiser, *Theory and Design of Charged Particle Beams*, Weinheim, Germany: WILEY-VCH Verlag, 2008, p. 149.

[28]  C. Li and R.A. Jameson, "Structure resonances due to space charge in periodic focusing channels", *Phys. Rev. Accel. Beams*, vol. 21, p. 024204, 2018. doi:10.1103/PhysRevAccelBeams.21.024204

[29]  I. Hofmann and O. Boine-Frankenheim, "Space-charge structural instabilities and resonances in high-intensity beam", *Phys. Rev. Lett.*, vol. 115, p. 204802, 2015. doi:10.1103/PhysRevLett.115.204802

[30]  D. Uriot and N. Pichoff, "Status of TraceWin Code", in *Proc. 6th Int. Particle Accelerator Conf. (IPAC'15)*, Richmond, VA, USA, May 2015, pp. 92–94. doi:10.18429/JACoW-IPAC2015-MOPWA008

[31]  R. De Maria *et al.*, "SixTrack V and runtime environment", *International Journal of Modern Physics A*, vol. 34, no. 36, p.1942035, 2019. doi:10.1142/S0217751X19420351

[32]  K. S. B. Li *et al.*, "Code Development for Collective Effects", in *Proc. 57th ICFA Advanced Beam Dynamics Workshop on High-Intensity and High-Brightness Hadron Beams (HB'16)*, Malmö, Sweden, Jul. 2016, pp. 362–367. doi:10.18429/JACoW-HB2016-WEAM3X01

[33]  A. Oeftiger and S. Hegglin, "Space Charge Modules for Py-HEADTAIL", in *Proc. 57th ICFA Advanced Beam Dynamics Workshop on High-Intensity and High-Brightness Hadron Beams (HB'16)*, Malmö, Sweden, Jul. 2016, pp. 124–129. doi:10.18429/JACoW-HB2016-MOPR025

[34] G. Franchetti and I. Hofmann, "Particle trapping by nonlinear resonances and space charge", *Nucl. Instrum. Methods Phys. Res., Sect A*, vol. 561, p. 195, 2006. doi:10.1016/j.nima.2006.01.031

[35] G. Franchetti and I. Hofmann, "Resonance trapping due to space charge and synchrotron motion, in theory, simulations, and experiments", in *Proc. 39th ICFA Advanced Beam Dynamics Workshop on High-Intensity and High-Brightness Hadron Beams (HB'06)*, Tsukuba, Japan, May-Jun. 2006, paper WEAX01, pp. 167–171.

[36] A. Oeftiger, "Animation of Space Charge Driven Parametric Resonance in 90 deg Stopband". doi:10.6084/m9.figshare.13562423.v1

[37] A. Burov, "Head-tail modes for strong space charge", *Phys. Rev. ST Accel. Beams*, vol. 12, p. 044202, 2009. doi:10.1103/PhysRevSTAB.12.044202

[38] V. Balbekov, "Transverse modes of a bunched beam with space charge dominated impedance", *Phys. Rev. ST Accel. Beams*, vol. 12, p. 124402, 2009. doi:10.1103/PhysRevSTAB.12.124402

[39] V. Kornilov and O. Boine-Frankenheim, "Head-tail instability and Landau damping in bunches with space charge", *Phys. Rev. ST Accel. Beams*, vol. 13, p. 114201, 2010. doi:10.1103/PhysRevSTAB.13.114201